ACOUSTICS 2012

Sonic Time Reversal Imaging optimization in reverberating, confined or noisy environments

E. Bavu, M. Melon, C. Auzou, S. Lobreau, C. Langrenne and A. Garcia

Conservatoire National des Arts et Métiers, 292 rue Saint-Martin 75141 Paris Cedex 03
eric.bavu@cnam.fr

Classical time-reversal (TR) imaging is based on the recording of the pressure field and its normal spatial derivative on a time-reversal mirror (TRM), followed by a numerical back-propagation of the time-reversed signals in a simulated propagation environment. In order to achieve accurate imaging, Green functions describing the environment must be well-known. When dealing with reverberating environments, precise numerical back-propagation is a rather complicated problem to solve. In order to avoid this situation, we propose a field separation method (FSM) in order to recover data that would be measured on the TRM in free-space, corresponding to the well-known free-field Green functions. This method consists in measuring the acoustic pressure on a double-layer semi-hemispherical TRM. Outgoing waves are separated from ingoing waves by using spherical-harmonic expansions. The outgoing contribution is then time-reversed and numerically back-propagated using the free-field propagators, allowing to achieve accurate imaging. This FSM also allows to separate contributions from sources outside the region of interest (ROI). This new method is illustrated by simulations and measurements in a confined car-trunk mock-up and in a reverberation room.

1 Introduction

Sonic time-reversal (TR) is a powerful method for the imaging and localization of sound sources, with high accuracy both in time and space domains [1, 2, 3]. TR imaging consists in reconstructing a time-reversed pressure field $p_{TR}(\vec{r}, t)$ by back-propagating in a simulated propagation the time-reversed signals measured on a TRM in the real medium. In order to achieve accurate imaging, the acoustic propagators must be well-known [1, 2]. When dealing with reverberating environments, precise numerical back-propagation is a rather complicated problem to solve. Other imaging techniques, such as nearfield acoustic holography and derivatives [4] are also not reliable in confined or reverberating environments. In order to overcome these problems with frequency domain imaging methods, several solutions have been proposed in literature [5, 6, 7]. In the present paper, we propose the use of a field separation method (FSM) based on spherical harmonic expansions in conjunction with TR imaging. Theory, numerical simulations and experimental results are included to illustrate the use of this modified TR imaging procedure.

2 Material and methods

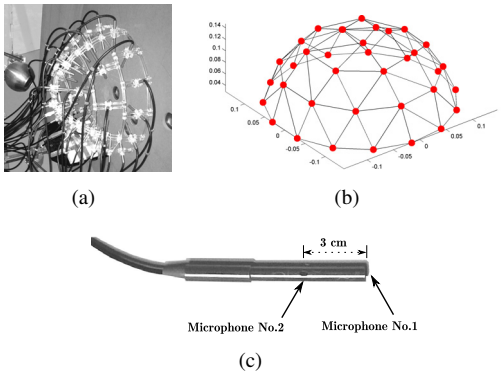

Figure 1: (a) Double-layered TRM in front of several baffled 5 cm diameter Aurasound® NSW2-326-8A in a reverberation room - (b) TRM geometry: red dots represent the position of each p-p probes - (c) p-p probe used in the TRM

In all measurements and numerical simulations presented in the following sections, the considered array is a double-layered hemispherical time-reversal mirror (Fig. 1) made-up of 36 phase and amplitude-calibrated pressure-pressure (p-p) probes (Fig. 1) manufactured by CTTM, thus giving access to 72 acoustic pressure measurements over time. The two hemispherical measurement layers formed by the p-p probes are spaced by 3 cm, the internal layer having a radius a_1 = 14.5 cm and the external layer having a radius a_2 = 17.5 cm.

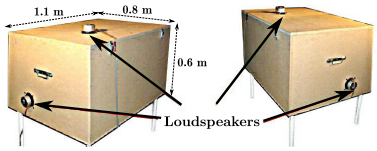

Figure 2: Outside views of the car trunk mock-up with Audax® HM130Z12 loudspeakers mounted on 5 of the 6 sides

Experimental results are shown for a car trunk mock-up and a reverberation room.

The car trunk mock-up is made of 22 mm Medium Density Fibreboard wood. Its shape is a nearly rectangular cuboid of $1.1 \times 0.8 \times 0.6$ m^3 (one side deviates of about 10° from verticality). Five 13 cm diameter Audax® HM130Z12 loudspeakers are mounted on five of the six sides (Fig. 2) .

The reverberation room in which the experiments are leaded is a right-angled trapezium-shaped room (surface: 20,8 m^2, volume: 63 m^3, reverberation duration $T_R \geq 4.5$ s).

The 72 synchronized time-pressure measurements are acquired and triggered through a N.I.® 96 channel PXI acquisition system, sampled at 32768 Hz and driven using Labview® software. The loudspeakers are driven by a computer using a M-Audio® 1010 PCI soundcard and Adobe® Audition® software. Calculation of TR imaging and acoustic field separation is achieved using Matlab® software. All calculations in the numerical simulation subsection are also achieved using Matlab® software.

3 Theoretical background

3.1 Sonic time-reversal imaging

In a weakly dissipative medium, the time-reversal procedure ensures that if an acoustic pressure field $p(\vec{r}, t)$ is solution of the wave equation, the time-reversed acoustic field $p(\vec{r}, -t)$ has a mathematical and physical existence. A time-reversed pressure field $p_{TR}(\vec{r}, t)$ can be reconstructed at position $\vec{r} \in (V)$ using a time-reversed version of the time domain Helmholtz-Kirchhoff equation (1) and measurements of the acoustic pressure and its normal derivative on points $\vec{s}$ on a surface (S) surrounding the volume (V) where the calculation is done to retrieve the pressure field:

$$p_{TR}(\vec{r}, t) = \iint_S \left(G(\vec{s}, \vec{r}; -t) * \frac{\partial p(\vec{s}; -t)}{\partial n_s} - \frac{\partial G(\vec{r}_s, \vec{r}; -t)}{\partial n_s} * p(\vec{s}; -t) \right) \cdot dS \quad (1)$$

The time-reversed field $p_{TR}(\vec{r},t)$ has the property to back-propagate to the acoustic sources positions and to reconstruct the time evolution of the radiated field at focal point, thus allowing to solve the inverse problem of acoustic field reconstruction and to locate and image acoustic radiating sources. Assuming the measurement is achieved in free-field conditions, the free-field Green functions are used in the calculations and the terms in the time domain Helmholtz-Kirchhoff equation (1) are detailed in the following system of equations (2), where $\cos(\gamma_s) = \dfrac{(\vec{s}-\vec{r}).\vec{n_S}}{|\vec{s}-\vec{r}|}$ and $\vec{n_S}$ is the normal vector to the measurement surface (S):

$$\begin{cases} G(\vec{s},\vec{r};-t) * \dfrac{\partial p(\vec{s};-t)}{\partial n_s} = \dfrac{1}{4\pi|\vec{s}-\vec{r}|} \times \dfrac{\partial p\left(\vec{s};-t-\dfrac{|\vec{s}-\vec{r}|}{c}\right)}{\partial n_s} \\ \dfrac{\partial G(\vec{r_s},\vec{r};-t)}{\partial n_s} * p(\vec{s};-t) = \dfrac{\cos(\gamma_s)}{4\pi|\vec{s}-\vec{r}|^2} \times p\left(\vec{s};-t-\dfrac{|\vec{s}-\vec{r}|}{c}\right) \\ \qquad\qquad + \dfrac{\cos(\gamma_s)}{4\pi c|\vec{s}-\vec{r}|} \times \dfrac{\partial p\left(\vec{s};-t-\dfrac{|\vec{s}-\vec{r}|}{c}\right)}{\partial t} \end{cases} \tag{2}$$

Equation (1) shows that in order to calculate the time-reversed field $p_{TR}(\vec{r},t)$, the acoustic field must be measured using monopolar and dipolar microphones. In our experiment, the double-layered hemispherical TRM allows to measure both $p(\vec{s},t)$ and its normal derivative using the two probes located at $\vec{s_1} \in (S_1)$ of radius a_1 and $\vec{s_2} \in (S_2)$ of radius a_2 using first order finite difference schemes:

$$\begin{cases} \dfrac{\partial p(\vec{s};-t)}{\partial n_s} \approx \dfrac{p(\vec{s_1};-t)-p(\vec{s_2};-t)}{a_2-a_1} \\ p(\vec{s};-t) \approx \dfrac{p(\vec{s_1};-t)+p(\vec{s_2};-t)}{2} \end{cases} \tag{3}$$

Since the acoustic field is not measured on a continuous surface (S) but rather space-sampled on this surface, the surface integral involved in equation (1) is replaced by a discrete sum in order to achieve time-reversal imaging using the measured data on the double-layered hemispherical TRM.

As stated in the previous paragraphs, TR *imaging* is based on the knowledge of the Green functions, which are the propagators in the measurement medium. In free-space-like environments such as an anechoic room, the analytic free-field Green functions are used to back-propagate the measured acoustic field and allow to obtain accurate and satisfying results [1]. However, when the medium is confined or reverberant, there is no analytic knowledge of the Green functions, which degrades the imaging process when not using the right acoustic propagators. This property is the great difference between TR *focusing*, where the back-propagation is achieved in the same medium than the propagation during measurements (the well known self-focusing property), and TR *imaging*, where the back-propagation is achieved in numerical model. On contrary to TR *imaging*, TR *focusing* has been shown to be more efficient in reverberating environments because reverberation enhances the measurement antenna aperture [8, 2]. In order to allow TR *imaging* in confined and reverberant environments, we propose the use of a field separation method (FSM), that suppress the contributions from noise sources that reside outside the ROI and "dereverberate" the acoustical measurements in order to achieve efficient TR imaging using free-field Green functions in confined or reverberant environments.

3.2 Field separation method

3.2.1 Pressure-pressure separation method

Previous published works show that separation methods can be used in spherical coordinates in order to recover free-field conditions [6, 9]. The proposed method is based on Weinreich *et al.* work [9] and involves spherical harmonics expansion. Based on the assumption that the TRM lays on a perfectly rigid surface, the pressure fields measured with the double-layered hemispherical antenna can be expressed using even spherical harmonics up to a maximum order N. The maximum order of expansion N is calculated from the number of probes in the TRM. With 36 p-p probes, the maximum order of decomposition is $N = 7$. In equation (4), $Y_n^m(\theta,\phi)$ are the normalized spherical harmonic functions, and $\mathcal{TF}^{-1}$ is the inverse Fourier transform operator:

$$\begin{cases} p(a_1,\theta,\phi,t) = \mathcal{TF}^{-1}\left(\displaystyle\sum_{n=0}^{N}\sum_{\substack{m=-n \\ (m+n)\text{even}}}^{+n} \hat{\alpha}_{nm} Y_n^m(\theta,\phi) e^{i\omega t}\right) \\ p(a_2,\theta,\phi,t) = \mathcal{TF}^{-1}\left(\displaystyle\sum_{n=0}^{N}\sum_{\substack{m=-n \\ (m+n)\text{even}}}^{+n} \hat{\beta}_{nm} Y_n^m(\theta,\phi) e^{i\omega t}\right) \end{cases} \tag{4}$$

In equation (4), the $\hat{\alpha}_{nm}$ and $\hat{\beta}_{nm}$ are complex coefficients that can be calculated from measured pressures by expansion using orthonormal properties of Y_n^m. As shown in equation (5), this formulation can be rewritten in terms of diverging waves (represented by spherical Hankel functions of second kind $h_n^{(2)}$) and standing waves (represented by spherical Bessel functions of first kind j_n):

$$\begin{cases} p(a_1,\theta,\phi,t) = \mathcal{TF}^{-1}\left(\displaystyle\sum_{n=0}^{N}\sum_{\substack{m=-n \\ (m+n)\text{even}}}^{+n} \left(\hat{a}_{mn} h_n^{(2)}(ka_1) + \hat{b}_{mn} j_n(ka_1)\right) Y_n^m(\theta,\phi) e^{i\omega t}\right) \\ p(a_2,\theta,\phi,t) = \mathcal{TF}^{-1}\left(\displaystyle\sum_{n=0}^{N}\sum_{\substack{m=-n \\ (m+n)\text{even}}}^{+n} \left(\hat{a}_{mn} h_n^{(2)}(ka_1) + \hat{b}_{mn} j_n(ka_1)\right) Y_n^m(\theta,\phi) e^{i\omega t}\right) \end{cases} \tag{5}$$

The $\hat{a}_{mn}$ and $\hat{b}_{mn}$ are the complex unknown quantities of the problem, $\hat{a}_{mn}$ being the unknown of interest in our problem in order to achieve dereverberating and denoising of measured pressures on the TRM. Solving this set of linear equations using systems (4) and (5) for $k(a_2 - a_1) \ll 1$ gives access to the knowledge of the constants $\hat{a}_{mn}$ and allows to compute the outgoing fields $p_{out}(a_{1,2},\theta,\phi,t)$ which correspond to the set of data that would have been measured in an semi-anechoic environment and that filter the contribution coming from zones located outside the ROI. These outgoing fields are then taken as entries for the time-reversal imaging process described in the previous subsection. As a consequence, the TR-FSM imaging method allows acoustic imaging of radiating sources in the ROI delimited by the double-layered hemispherical TRM and allows to achieve measurements in non anechoic environments without degrading the TR imaging process using free-field Green functions.

3.2.2 Pressure-velocity separation method

Similarly to the pressure-pressure separation method, it is possible to achieve pressure-velocity separation, based on analogous assumptions and arguments. Using the measurement pressures on both layers of the TRM $p(a_1,\theta,\phi,t)$ and $p(a_2,\theta,\phi,t)$, the pressure $p(a,\theta,\phi,t)$ and normal particular

velocity $v(a,\theta,\phi,t)$ at mean radius $a = \frac{a_1+a_2}{2}$ can be computed using first order finite difference schemes:

$$\begin{cases} p(a,\theta,\phi,t) \approx \dfrac{p(a_1,\theta,\phi,t)+p(a_2,\theta,\phi,t)}{2} \\ v(a,\theta,\phi,t) \approx \mathcal{TF}^{-1}\left(\dfrac{\mathcal{TF}\left(p(a_2,\theta,\phi,t)-p(a_1,\theta,\phi,t)\right)}{i\omega\rho\,(a_2-a_1)}\right) \end{cases} \quad (6)$$

Based on the assumption that the TRM lays on a perfectly rigid surface, these approximated pressure and velocity fields (Eq.(6)) can be expanded onto even spherical harmonics:

$$\begin{cases} p(a,\theta,\phi,t) = \mathcal{TF}^{-1}\left(\sum_{n=0}^{N}\sum_{\substack{m=-n \\ (m+n)\text{even}}}^{+n} \hat{\delta}_{nm} Y_n^m(\theta,\phi)e^{i\omega t}\right) \\ v(a,\theta,\phi,t) = \mathcal{TF}^{-1}\left(\sum_{n=0}^{N}\sum_{\substack{m=-n \\ (m+n)\text{even}}}^{+n} \hat{\epsilon}_{nm} Y_n^m(\theta,\phi)e^{i\omega t}\right) \end{cases} \quad (7)$$

As shown in equation (8), this formulation (Eq.(7)) can be rewritten in terms of diverging waves (represented by spherical Hankel functions of second kind $h_n^{(2)}$) and standing waves (represented by spherical Bessel functions of first kind j_n):

$$\begin{cases} p(a,\theta,\phi,t) = \mathcal{TF}^{-1}\left(\sum_{n=0}^{N}\sum_{\substack{m=-n \\ (m+n)\text{even}}}^{+n} \left(\hat{a}_{mn}h_n^{(2)}(ka)+\hat{b}_{mn}j_n(ka)\right)Y_n^m(\theta,\phi)e^{i\omega t}\right) \\ v(a,\theta,\phi,t) = \mathcal{TF}^{-1}\left(\sum_{n=0}^{N}\sum_{\substack{m=-n \\ (m+n)\text{even}}}^{+n} \dfrac{\left(\hat{a}_{mn}h_n^{(2)\prime}(ka)+\hat{b}_{mn}j_n{}'(ka)\right)Y_n^m(\theta,\phi)e^{i\omega t}}{i\rho c}\right) \end{cases} \quad (8)$$

Solving this set of linear equations using systems (7) and (8) gives access to the knowledge of the constants $\hat{a}_{mn}$ and allows to compute the outgoing fields $p_{out}(a_{1,2},\theta,\phi,t)$ which correspond to the set of data that would have been measured in an anechoic environment and that filter the contribution coming from zones located outside the ROI. These outgoing fields are then taken as entries for the time-reversal imaging process described in the previous subsection. As a consequence, the TR-FSM imaging method allows acoustic imaging of radiating sources in the ROI delimited by the double-layered hemispherical TRM and allows to achieve measurements in non anechoic environments without degrading the TR imaging process using free-field Green functions.

3.2.3 Frequency range of validity

For both p-p and p-v separation methods, the maximum order N of expansion onto spherical harmonics is fixed to $N = 7$ since the TRM is composed of 36 probes. Equations (5) and (8) are valid if the adimensional number $ka_2 \leq N$, which gives access to a cut-off frequency $f_c \approx 2180$ Hz for $a_2 = 0.175$ m. This cut-off frequency could be higher with a smaller antenna or with an antenna with a larger number of probes, giving access to higher order of expansions onto spherical harmonics. As a consequence, in all experiments and numerical simulations in the following, the signals emitted by acoustic sources are chosen to be bounded to this frequency range.

4 Results and Discussion

4.1 Comparison between p-p and p-v separation: numerical simulations

In this section, we present numerical simulations results showing the ability of TR-FSM to successfully image and localize acoustic sources in the ROI under the TRM, when perturbed by noise sources outside the ROI, both in free space and confined environments. As we presented both p-p separation and p-v separation in the previous section, these numerical simulations will provide insights about the efficiency of both separation methods when used for TR-FSM imaging. In the following, the reconstruction quality and field separation efficiency is evaluated and quantified using the following numerical indicator I_n (see Eq. (9)):

$$I_n = 20\log_{10}\left(\frac{1}{S_{ROI}}\iint_{S_{ROI}} \frac{\sqrt{\left\langle\left(p(x,y,t)-p^{ref}(x,y,t)\right)^2\right\rangle_t}}{p_{RMS}^{ref}(x,y)}dxdy\right) \quad (9)$$

where S_{ROI} is the surface of the ROI on which the TR back-propagation is calculated, $p(x,y,t)$ is the back-propagated field, $p^{ref}(x,y,t)$ is the back-propagated field in free-field conditions without perturbating sources, and $p_{RMS}^{ref}(x,y)$ its root-mean-square (RMS) value.

I_n evaluates both in time and space domains the reconstruction quality of the TR field in the ROI, and increases if any error occurs in phase, amplitude, or spatial localization. Lower values of I_n indicates better reconstructions.

4.1.1 Separation from noise sources outside the ROI

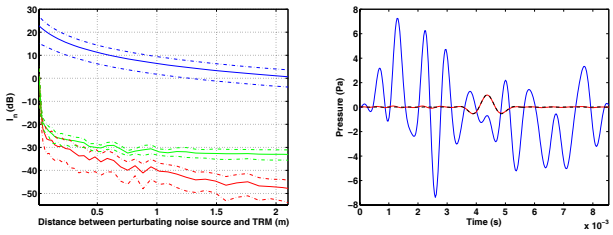

(a) (b)

Figure 3: (a) Reconstruction quality of TR imaging when perturbed by a noise source at a varying distance d from TRM; Blue: without separation; Green: with p-v separation; Red: with p-p separation - Dotted colored lines indicate the 68 % spatial confidence interval for I_n - (b) Blue: Pressure on microphone No. 24 in presence of noise source at 5 cm from TRM; Red: Pressure computed from measured data using p-p separation; Black dotted: pressure measured without perturbating noise source

Figure 3 shows numerical simulations results obtained for the imaging of a ROI-centered acoustic source in presence of a noise source outside the ROI, at a distance d from the TRM. The noise source emits a filtered white noise (band-pass: [0 – 2180] Hz) and the source in the ROI emits an impulsive signal (Hanning windowed spectrum, from 0 Hz to 1800 Hz) in order to simulate severe measurement conditions. The perturbating noise source has a pressure level of 12 dB higher than the source in the ROI.

Figure 3(a) shows reconstruction quality indicator I_n when TR only is used (blue), TR-FSM with pressure-pressure is used (red) and TR-FSM with pressure-velocity is used (green). The first striking result is that both p-p and p-v separation are

very efficient at suppressing the acoustic perturbation coming from outside the ROI, allowing to improve the reconstruction quality indicator of at least 22 dB for $d = 0.005$ m, even if the perturbating noise source has a higher level that the source of interest. Furthermore, this study shows that for all distances, p-p separation is more efficient than p-v separation, strongly improving the reconstruction indicator I_n. This result can be interpreted by the fact that p-v separation involves an approximation of the velocity field using first-order finite difference schemes, which can degrade slightly the obtained separation, especially for medium and high frequencies. This result is also confirmed by the fact that I_n for p-v separation meets an horizontal asymptote, signifying that this separation cannot be better because of the velocity approximation achieved in this method. On the contrary, for this experiment, p-p separation does not seem to meet any horizontal asymptote and improves greatly the separation achieved and the imaging obtained using TR-FSM.

Figure 3(b) confirms that p-p separation is a very efficient way of suppressing the acoustic contributions from sources outside the volume delimited by the TRM, even for close sources from the TRM at high levels. The p-p separated acoustic field on the TRM (red line) is almost perfectly superimposed to the field that would have been measured in half space without perturbating noise (black dotted-line), although the contribution of the acoustic of interest seems entirely masked by the perturbating noise source when no separation is achieved (blue line).

4.1.2 Simulations in a confined environment

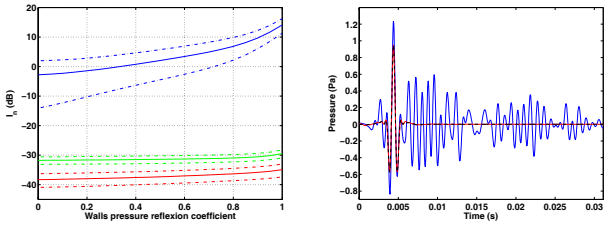

(a) (b)

Figure 4: (a) Reconstruction quality of TR imaging in a confined shoebox with a varying wall pressure reflection coefficient r in presence of a perturbating noise source. Blue: without separation; Green: with p-v separation; Red: with p-p separation - Dotted colored lines indicate the 68 % spatial confidence interval for I_n - (b) Blue: Pressure on microphone No. 24 in presence of noise source at 5 cm from TRM with $r = 0.95$; Red: Pressure computed from measured data using p-p separation; Black dotted: field pressure measured without perturbating noise source and without reverberation

In order to test TR-FSM imaging performances in confined environments, a similar numerical simulation has been performed in a confined rectangular cuboid of $1.1 \times 0.8 \times 0.6$ m^3 "shoebox" approaching the car trunk mock-up geometry used in experimental procedures. Figure 4 shows numerical simulations results obtained for the imaging of a ROI-centered acoustic source in presence of a noise source outside the ROI, located at 5 cm from the shoebox corner and 10 cm from TRM. The noise source emits a filtered white noise (bandpass: $[0-2180]$ Hz) and the source in the ROI emits an impulsive signal (Hanning windowed spectrum, from 0 Hz to 1800 Hz). The perturbing noise source has the same pressure level as the source in the ROI. The reverberated field originating from the reflections on the walls has been calculated using the source-image method proposed by Allen *et al.* [10]. In these calculations, the wall pressure reflection coefficients are changed from 0 (perfectly anechoic case) to 1 (perfectly reflective case) for 5 of the 6 walls, in order to observe the efficiency of p-p and p-v separation in confined and reverberant environments. The wall on which is laying the TRM is kept perfectly reflective, thus respecting the assumption of even spherical harmonics decomposition.

Figure 4(a) shows reconstruction quality indicator I_n when TR only is used (blue), when p-p TR-FSM is used (red) and when p-v TR-FSM is used (green), for each wall pressure reflection coefficients. The conclusions which can be drawn from the analysis of these results meet those obtained in the previous subsection: p-p and p-v separation are both efficient at suppressing the acoustic perturbations coming from outside the ROI (noise source and reverberation), allowing to improve the reconstruction quality indicator even for small, confined and strongly reflective environments. For all reflection coefficients, p-p separation appears again to be more efficient than p-v separation, strongly improving the reconstruction indicator I_n.

Figure 4(b) confirms that p-p separation is a very efficient method to suppress the acoustic contributions from noise sources placed outside the volume delimited by the TRM and dereverberating data measured on the TRM, even for highly reverberant and confined environments. The p-p separated acoustic field on the TRM (red line) is almost perfectly superimposed to the field that would have been measured in free space without perturbating noise (black dotted-line), almost completely suppressing the contribution of the perturbating noise source and reflections on the boundaries of the shoebox, observed when no separation is achieved (blue line).

4.2 Experimental results

In the previous section, we have shown that TR-FSM is a powerful and efficient imaging method when confronted to noisy and confined environments. This section presents some experimental results obtained in a car trunk mock-up and a reverberation room in order to show the improvement when performing sonic sources imaging in these situations.

4.2.1 Source localization and imaging accuracy

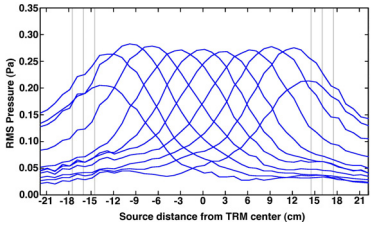

Figure 5: Source localization using TR-FSM imaging - Blue line: RMS pressure obtained after back-propagation for several sources positions - Vertical gray lines: indicative radii of TRM layers

Non-modified sonic TR imaging is known to be an efficient and precise imaging and localization tool in free space [1, 3]. This subsection shows that the modified TR-FSM procedure also achieves high quality spatial localization of sound sources and does not degrades the spatial reconstruction of the imaged sources. Figure 5 shows RMS pressure

obtained on a diameter dimension of the ROI for several 3 cm spaced positions of a baffled loudspeaker. These graphics correspond to transverse cuts of RMS pressure maps obtained in the ROI. The loudspeaker studied in this part is a 5 cm diameter Aurasound® NSW2-326-8A loudspeaker in the ROI (see Fig. 1(a)). Each measurement shows a well localized source position. Interestingly, for positions approaching the TRM, the amplitude of the reconstructed pressure field appears to reduce. This can be explained by the fact that for these positions, part of the loudspeaker was placed between the two layers of the TRM, thus leading to partial separation of the measured acoustic field.

4.2.2 Acoustic sources in a car trunk mock-up

Figure 6 shows the imaging results obtained in the car trunk mock-up described in section 2 (Fig.2), with an Audax® HM130Z12 loudspeaker placed in the ROI, and 3 similar loudspeakers outside of the ROI acting simultaneously as perturbing sources in this confined environment. The source of interest emits an impulsive signal (Hanning windowed spectrum, from 0 Hz to 2050 Hz), and the 3 perturbing sources emit uncorrelated white noises. Without the use of FSM (Fig. 6(a)), the obtained RMS pressure image is completely masked by the perturbing noise source and reverberation contributions. The use of TR-FSM (Fig. 6(b)) allows to retrieve the exact position and level of the loudspeaker placed in the ROI.

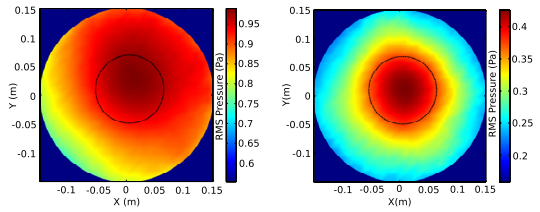

(a) (b)

Figure 6: TR imaging (a) and TR-FSM imaging (b) obtained in the car trunk mock-up with 3 perturbing sources - Black-dotted line indicates the position and size of the loudspeaker in the ROI

4.2.3 Acoustic sources in a reverberation room

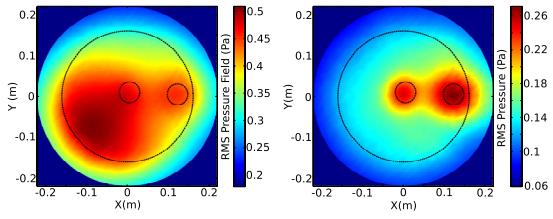

(a) (b)

Figure 7: TR imaging (a) and TR-FSM imaging (b) obtained in a reverberation room for two sources placed in the ROI and one perturbing source - Black-dotted line indicate positions and sizes of the two loudspeakers and the TRM position and size.

Similar experiments have been conducted in the reverberation room described in section 2, also demonstrating the efficiency of TR-FSM when measurements are performed in a noisy and/or reverberant environment. Figure 7 shows the imaging results obtained in the reverberation room, with two baffled Aurasound® NSW2-326-8A loudspeakers in the ROI and emitting simultaneously uncorrelated signals: the source located at the center of the ROI emits an impulsive signal (Hanning windowed spectrum, from 0 Hz to 2800 Hz), and the source located at the right of the ROI emits a white noise signal. Another loudspeaker is acting as a perturbing source outside of the ROI emitting a low frequency impulsive signal (Hanning windowed spectrum, from 0 Hz to 750 Hz). Similarly to what is observed in the car trunk mock-up, without the use of FSM (Fig. 7(a)), the obtained RMS pressure image is mostly masked by the perturbing noise source and reverberation contributions. The use of TR-FSM (Fig. 7(b)) allows to retrieve the exact position and level of the two loudspeakers in the ROI.

5 Conclusion

In this study, we presented a new modified sonic time-reversal imaging method using a field separation method based on spherical harmonics expansions and the use of a specifically developed double-layered hemispherical TRM. The theory of this new imaging technique has been detailed. Numerical simulations and experimental measurements show that TR-FSM is a powerful and precise imaging method, keeping the advantages of classical TR imaging, but improving its accuracy in noisy, confined or reverberant environment. We also show that p-p separation method is more precise and efficient than p-v separation with our double layer p-p TRM, especially for medium and high frequency contents. Experimental results in a car trunk mock-up and a reverberant room in presence of perturbating noise sources show that this new modified TR procedure is very efficient and has many potential practical applications.

References

[1] E. Bavu, A. Berry, "Super-resolution imaging of sound sources in free field using a numerical time-reversal sink", *Acta Acust. United Ac.*, **95** (4), 595-606 (2009)

[2] M. Fink, D. Cassereau, A. Derode, C. Prada, P. Roux, M. Tanter, J-L. Thomas, F. Wu, "Time reversed acoustics", *Rep. Prog. Phys.* **63**, 1933-1995 (2000)

[3] S.G. Conti, P. Roux, W.A. Kuperman, "Near-field time-reversal amplification", *J. Acoust. Soc. Am.* **121** (6), 3602–3606 (2007)

[4] S. F. Wu, "Methods for reconstructing acoustic quantities based on acoustic pressure measurements", *J. Acoust. Soc. Am.* **124** (5), 2680-2697 (2008)

[5] F. Jacobsen, V. Jaud, "Statistically optimized near field acoustic holography using an array of pressure-velocity probes" *J. Acoust. Soc. Am.* **121**(3), 1550–1558 (2007)

[6] M. Melon, C. Langrenne, P. Herzog, A. Garcia, "Evaluation of a method for the measurement of subwoofers in usual rooms," *J. Acoust. Soc. Am.* **127** (1), 256–263 (2010)

[7] M. Aucejo, N. Totaro, J.-L. Guyader, "Identification of source velocities on 3D structures in non-anechoic environments: Theoretical background and experimental validation of the inverse Patch Transfer Functions method", *Journal of Sound and Vibration*, **329**(18), 3691-3708, 2010

[8] E. Bavu, C. Besnainou, V. Gibiat, J. de Rosny, M. Fink, "Subwavelength Sound Focusing Using a Time-Reversal Acoustic Sink", *Acta Acust. United Ac.* **93** (5), 706-715 (2007)

[9] G. Weinreich, E. B. Arnold, "Method for measuring acoustic radiation fields", *J. Acoust. Soc. Am.* **68**, 404–411 (1980)

[10] J.B. Allen, D.A. Berkley, "Image method for efficiently simulating small-room acoustics", *J. Acoust. Soc. Am.* **65**(4), 943–950 (1979)